HPM-14, a New Germanosilicate Zeolite with Interconnected Extra-Large Pores Plus Odd-Membered and Small Pores

Zihao Rei Gao[†], Jian Li[‡⋆], Cong Lin[‖], Alvaro Mayoral[⊥], Junliang Sun[‡], and Miguel A. Camblor[†⋆]

[†] *Instituto de Ciencia de Materiales de Madrid, Consejo Superior de Investigaciones Científicas (ICMM-CSIC), c/Sor Juana Inés de la Cruz 3, Madrid 28049, Spain*

[‡] *College of Chemistry and Molecular Engineering, Beijing National Laboratory for Molecular Sciences, Peking University 5 Yiheyuan Road, Beijing, 100871, China and Berzelii Center EXSELENT on Porous Materials, Department of Materials and Environmental Chemistry Stockholm University, Stockholm, 10691, Sweden*

[‖] *School of Advanced Materials Peking University, Shenzhen Graduate School, Shenzhen, 518055, China*

[⊥] *Laboratorio de Microscopias Avanzadas (LMA), Instituto de Ciencia de Materiales de Aragon (ICMA-CSIC), Univesidad de Zaragoza c/ Mariano Esquillor, Edificio I+D, 50180, Zaragoza, Spain and Center for High-resolution Electron Microscopy (ChEM), School of Physical Science and Technology ShanghaiTech University, 393 Middle Huaxia Road, Pudong, Shanghai, 201210, China*

Correspondence: jian.li@mmk.su.se; macamblor@icmm.csic.es

Abstract

HPM-14 is a new extra-large pore zeolite synthesized using imidazolium-based organic structure-directing agents, fluoride anions and germanium and silicon as tetrahedral components of the framework. Due to the presence of stacking disorder, the structure elucidation of HPM-14 was challenging, and different techniques were necessary to clarify the details of the structure and to understand the nature of the disorder. The structure has been solved by three-dimensional electron diffraction technique (3D ED) and consists of an intergrowth of two polymorphs possessing a three-dimensional channel system, including an extra-large pore opened through windows made up of sixteen tetrahedral atoms (16-membered ring, 16MR) as well as two additional sets of odd-membered (9MR) and small (8MR) pores. The intergrowth has been studied by scanning transmission electron microscopy (C_s-STEM) and powder X-ray diffraction simulations (DIFFaX), which show a large predominance of the monoclinic polymorph A.

Zeolites continue to attract scientists searching for new structures and applications.[1] While around half a dozen new zeolite framework types are approved each year by the International Zeolite Association (IZA),[2] the discovery of new zeolite structures and their structural characterization are still very far from routine. For the discovery, we still rely much on trial and error experiments based on a handful concepts derived from the experience accumulated in the last eight decades or so.[3] The so-called "structure-directing effects", including the use of organic structure-directing agents (OSDA) of various types,[4,5] different mineralizers (fluoride or hydroxides),[6] different heteroatoms (atoms other than Si or Al)[7] and other factors such as concentration of the synthesis mixture,[8] can be used in the design of synthesis experiments aimed to obtaining new zeolites. Among the known zeolites, extra-large pores (i.e. pores opened through windows made up of more than 12 tetrahedra) and odd-membered pores are still relatively rare, and very scarcely combined: only two interrupted frameworks (-IRY and *-EWT),[9] and one true, i.e. non-interrupted zeolite framework (GeZA)[10] combine large and odd pores. For the structure elucidation, new techniques, especially electron crystallography techniques,[11] have been developed lately that are proving extremely useful in extracting and processing single-crystal-like information from very tiny crystallites, even for impure powder samples. However, materials with structural disorder, such as stacking faults, are particularly difficult to elucidate in all their details and often require combining different techniques. Zeolite beta is a famous case in which electron diffraction (ED) patterns and high-resolution transmission electron microscopy (HRTEM) images were used complementarily to construct possible models. These models were then validated by simulating the corresponding powder X-ray diffraction (PXRD) patterns.[12] The program DIFFaX, which is now regularly used to simulate PXRD patterns of structural models containing stacking faults, was initially developed to characterize zeolite beta.[13] Here, we present HPM-14, a new, fully connected zeolite with extra-large 16MR pores plus additional odd-membered 9MR and small 8MR pores, whose synthesis is based on the combined use of imidazolium-based organic structure-directing agents, fluoride anions and germanium together with silicon as fundamental tetrahedral atoms. Because it consists of an intergrowth of two polymorphs, the structure of HPM-14 was solved by 3D ED methods and the nature of disorder was studied by spherical aberration corrected scanning transmission electron microscopy (C_s-STEM) and powder x-ray diffraction simulations (DIFFaX), which show a large predominance of one of the polymorphs, the monoclinic polymorph A.

For the discovery of HPM-14, two easily synthesized OSDAs (Scheme S1) and a series of high-throughput experiments were performed (Tab. S1). With OSDA1, i.e. 1-methyl-3-(2',4',6'-trimethylbenzyl)imidazolium, zeolite HPM-14 could be synthesized from a gel with composition 0.7 SiO_2 : 0.3 GeO_2 : 0.5 OSDAOH : 0.5 HF : 5 H_2O under rotation at 160 °C for 5-9 days (Entries 6a-6c, Tab. S1). OSDA2, i.e. 1,1'-((2,4,6-trimethyl-1,3-phenylene)bis(methylene))bis(3-methylimidazolium), was also studied under a more limited range of conditions, yielding a pure and well crystallized phase from a gel composition 0.4 SiO_2 : 0.6 GeO_2 : 0.4 OSDA(OH)2 : 0.8 HF : (4-5) H_2O under rotation at 160 °C for 5-7 days. See Supporting Information for more zeolite synthesis details and discussion.

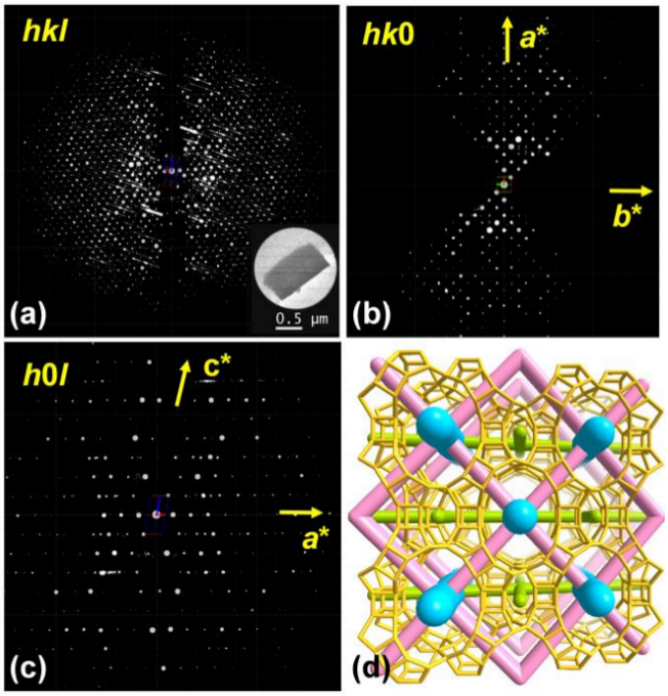

Figure 1: Reconstructed 3D cRED data of HPM-14 indexed with monoclinic symmetry: (a) overview, and selected planes in the reciprocal lattice corresponding to (b) *hk0* and (c) *h0l*. Owing to the streak along a* for *hkl: l = 2n + 1* reflections, some reflections violate the reflection conditions deduced (see text); (d) The multichannel system in HPM-14: one 16MR (blue), two 8MR (green) and two 9MR (pink).

Continuous rotation electron diffraction (cRED) data of as-made HPM-14 were collected (Tab. S2) and the 3D reciprocal lattice was reconstructed using REDp software.[11a] The cRED data were indexed directly in a monoclinic unit cell: 23.57 Å, 24.35 Å, 10.51 Å, 90.09°C, 100.78°C, 90.26°C (Figure 1a). From the 2D slices cut from the 3D reciprocal lattice, we could deduce the reflection conditions to be *hk0: h + k = 2n, h0l: h = 2n, h00: h = 2n* (Figure 1b, 1c). Three space groups, *C2*, *Cm*, *C2/m*, were found possible after analysis of the reflection conditions. Considering that most zeolite frameworks in the Database of Zeolite Structures are centrosymmetric,[2] the cRED data was processed with fixed unit cell and space group *C2/m* (the highest symmetry) using XDS program.[14] The monoclinic structure model of HPM-14 (named HPM-14A) was then solved from cRED data by using the dual-space algorithm of ShelxT.[15] Ten unique T atoms (T = Si, Ge) and part of O atoms could be located directly. Missing O atoms were added between the T atoms based on the chemical knowledge of zeolites. However, there were a lot of streaks along a* axis for *hkl: l = 2n + 1* reflections in the reconstructed 3D reciprocal lattice, which strongly suggested the existence of stacking faults. ED patterns under different tilt angle during cRED data collection confirmed the stacking faults (Fig. S1). After removing the streaks in 3D reciprocal lattice (Fig. S2a, S2b), an orthorhombic unit cell, with 24.26 Å, 10.49 Å, 23.98 Å, 90.72°C, 90.22°C, 90.08°C can be obtained. The new 2D slices based on the orthorhombic symmetry were cut from 3D reciprocal lattice using REDp, which suggested possible space

group *P2na* and *Pmna* (reflection condition: *h0l: h + l = 2n, hk0: h = 2n*; Fig. S2c, S2d). Then, the cRED data were re-processed with the orthorhombic unit cell and space group Pmna using XDS program again. The orthorhombic structure model of HPM-14 (HPM-14B) was outputted with the same unique T atoms and O atoms as HPM-14A by ShelxT. In order to facilitate the description of the structure of HPM-14A and HPM-14B, we rearranged the unit cell parameters of HPM-14B with non-standard space group *Pbmn* (Permutation: *c*, *a*, *b*). Then, the unit cell parameters were refined by Lebail fitting of the powder diffraction data of a calcined sample, which resulted in 22.9931(1) Å, 24.1974(5) Å, 10.3468(5) Å, 90°C, 100.230(9)°C, 90°C for HPM-14A (Fig. S3), and 22.64034 Å, 24.18114 Å, 10.66045 Å, 90°C, 90°C, 90°C for HPM-14B (Fig. S4). Finally, the structure was optimized by distance least-squares refinement using the program DLS-76.[16]

The channel system of HPM-14 is 3D with intersecting 16+8 x 9+8 x 9 MR. The 16MR and one of the 8MR channels are 1D along [001] direction (Figure 1d). These are connected in the perpendicular directions through 9MR windows forming a 2D undulating channel and through 8MR windows forming a 1D straight channel. This results into an interconnected 3D pore system with pore apertures of 12.3 x 8.6 Å(16MR), 5.6 x 3.7 Å(9MR), 5.4 x 1.9 Å(8MR along *c*-axis), and 4.6 x 3.9 Å(8MR along *a*-axis), respectively (Fig. S5). The stacking faults do not fundamentally affect the porosity of HPM-14. The framework of HPM-14 shows some similarity but significant differences to the SOF framework (SU-15 zeolite).[17] Both structures have the *t-sof-2*, i.e. $[4^4.5^6.9^2]$ and the *d4r*, i.e. $[4^6]$ (Figure 2a) tilings and may be built using a chain that contains the $[4^4.5^6.9^2]$ tilings. However, neighboring $[4^4.5^6.9^2]$ tilings are related by an inversion point in SOF-chain (Figure 2g) and by a mirror plane in HPM-14-chain (Figure 2b). This converts the 12MR channel in SOF into a 16MR plus an 8MR channel in HPM-14. Then, HPM-14-layers (Figure 2c) and SOF-layers (Figure 2h) are formed by connection of consecutive HPM-14-chains or SOF-chains, related by a glide plane, along the [100] direction. Successive layers are connected by *d4r*s to form the 3D framework of HPM-14 or SOF. The differences between HPM-14A and HPM-14B are related to the way successive chains are connected along the *a*-axis. When chains connect always at the same side an AAAA packing results in the monoclinic HPM-14A (Figure 2e), while connecting at alternating sides yields the ABAB packing of the orthorhombic HPM-14B (Figure 2f). The packing of HPM-14A is similarly to that of SOF (Figure 2i), also monoclinic. We predict that, similar to HPM-14, an orthorhombic variant of SOF might exist, although there are no signs of intergrowths in the actual SU-15 zeolite.[17]

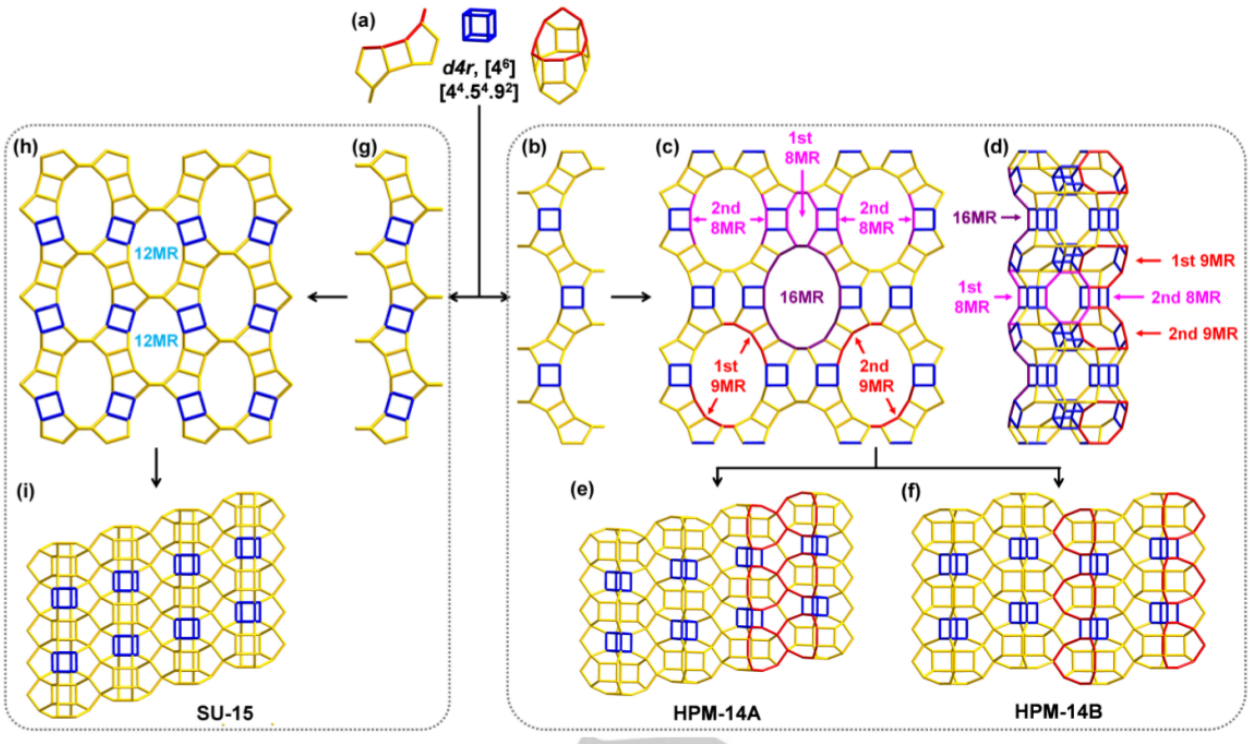

Figure 2: Structure description of HPM-14 and SOF: (a) *d4r* and $[4^4.5^6.9^2]$ tilings, (b) HPM-14-chain formed by mirror plane operation, (c) HPM-14-layer along [001], (d) two consecutive HPM-14-chains showing the 9 and 8 MR pores running in the plane normal to [001], (e) HPM-14A along [010], showing AAAA packing, (f) HPM-14B along [010], showing ABAB packing, (g) SOF-chain formed by inversion symmetry operation, (h) SOF-layer along [001], and (i) SOF along [010], showing AAAA packing. Only T-atom connections are shown; highlighted T-atoms: violet (16MR), red (9MR), pink (8MR) and blue (*d4r*).

The stacking faults described are fully supported by selected area electron diffraction (SAED) data, which show diffuse scattering patterns in the low-order zone axis more clearly than the cRED data. SAED patterns along the [010] direction show that all reflections with $l = 2n$ are sharp (Figure 3b), while reflections with $l = 2n + 1$ appear as streaks along a^* direction. This indicates stacking disorder along the direction parallel to a^* with layers translated by $\pm 1/2c$. The absence of streaks along [100] and [001] (Figure 3a, 3c), indicates that there is no disorder in the projection along the a- and c- axes.

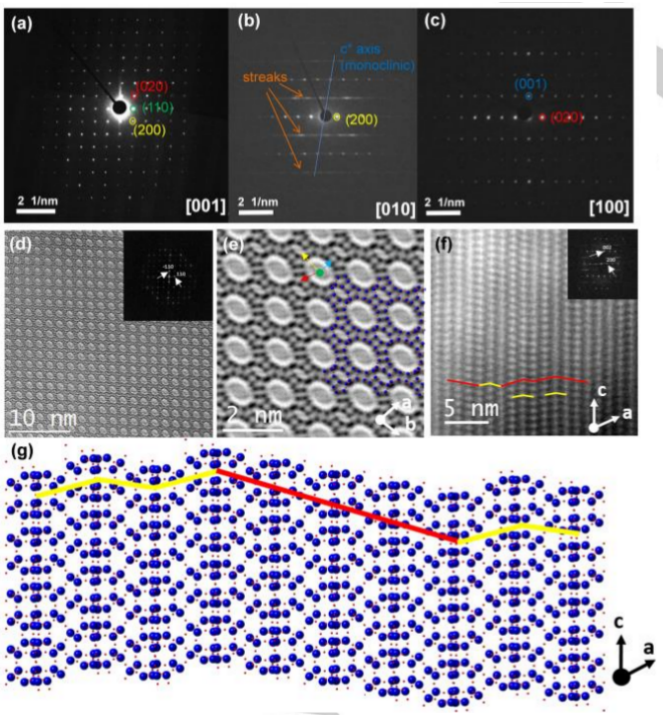

Figure 3: C_s-corrected STEM analysis of HPM-14. SAED patterns along (a) [001], (b) [010] showing diffuse streaks, (c) [100]. (d) ABF high-resolution image of the framework along [001]. (e) A closer look allows the visualization of the extra-large pores (green dot) and smaller rings (marked by yellow, red and blue arrows for 8, 5 and 4 MRs, respectively). (f) High-resolution micrograph along [010]. (g) Schematic model with the Si and O (blue and red spheres, respectively). In (d) and (f), the FD is presented in the inset; in (f) and (g) the stacking sequence has been marked with red and yellow lines denoting monoclinic and orthorhombic domains, respectively.

Electron Microscopy analysis was performed by means of spherical aberration corrected (C_s-corrected) Scanning Transmission Electron Microscopy (STEM) with an annular dark field/bright field detector (ADF/ABF). Figure 3d displays the C_s-corrected STEM-ABF image along the [001] orientation, where the oval shaped large pores are clearly visualized. The Fourier diffractogram (FD, inset) can be indexed in the *C2/m* space group. A closer inspection of the framework (Figure 3e) allows the visualization of the 16MRs surrounded by 8, 5 and 4 MRs. On a crystal rotated 90° respect to the [001] direction the existence of a disordered structure is evidenced (Figure 3f). The resulting structure is predominantly monoclinic. A schematic model representing the existence of these stacking faults is depicted in Figure 3g. Fig. S6 shows the DIFFaX simulations of intergrown structures together with the experimental pattern of calcined HPM-14 (see Supporting Information for further details and discussion). The comparison reveals that HPM-14 is predominantly the monoclinic polymorph A, with around a 90% predominance. The major presence of HPM-14A is also proved by C_s-corrected STEM images (Fig. S7).

In conclusion, HPM-14 is a new germanosilicate zeolite with a three-dimensional system of pores including

extra-large 16MR pores of 12.3 x 8.6 Åfree aperture. This, together with small 8MR pores, runs along [001] direction, while in the perpendicular direction 8MR and 9MR pores exist. The zeolite was synthesized using two different types of imidazolium cations (one monocationic, the other dicationic) of facile synthesis. The structure, which has a very low framework density of 14.1 T/1000 $Å^3$, was solved by cRED which evidenced the existence of two intergrown polymorphs, one monoclinic (HPM-14A), the other orthorhombic (HPM-14B), due to stacking faults along [100] direction. The stacking faults does not block the extra-large pore and have little impact on the smaller pores that connect them, because the large pores are separated from each other by very small stretches of 8MR and 9MR pores. The intergrowth has been studied by C_s-corrected STEM and DIFFaX simulations of the XRD patterns, concluding a large predominance of the monoclinic polymorph HPM-14A.

Acknowledgments

The authors acknowledge financial support by the Spanish Ministry of Science, Innovation and Universities (project MAT2015-71117-R, MINECO/FEDER, UE), the National Natural Science Foundation of China (No. 21871009, 21621061, 21527803, 21471009, NFSC-21850410448, NSFC-21835002), the Swedish Research Council (VR) and the Knut and Alice Wallenberg Foundation (KAW), and the Centre for High-resolution Electron Microscopy (ChEM), supported by SPST of ShanghaiTech University under contract No. EM02161943. A.M. also acknowledges funding by the Spanish Ministry of Science, Innovation and Universities through the Ramon y Cajal Program (RYC2018-024561-I).

References

[1] a) A. Burton, *Catal. Rev. Sci. Eng.* **2018**, *60*, 1, 132-175; b) J. Shin, D. Jo, S.B. Hong, *Acc. Chem. Res.* **2019**, *52*, 5, 1419-1427.

[2] Ch. Baerlocher, L. B. McCusker, Database of Zeolite Structures: http://www.iza-structure.org/databases/, access on March 8th, 2020.

[3] a) C. S. Cundy, P. A. Cox, *Chem. Rev.* **2003**, *103*, 663-702; b) C. S. Cundy, Cox, P. A., *Microporous Mesoporous Mater.* **2005**, *82*,1-78.

[4] R. F. Lobo, S. I. Zones, M. E. Davis, *J. Incl. Phenom.Macrocycl. Chem.* **1995**, *21*, 47-78.

[5] Insights into the Chemistry of Organic Structure-directing Agents in the Synthesis of Zeolitic Materials, Vol. 175 (Eds.: L. Gómez-Hortigüela), Springer, 2018.

[6] a) E. M. Flanigen, R. L. Patton, U.S. Patent 4, 073, 865, **1978**; b) Hydrothermal Chemistry of Zeolites (Eds.: R. M. Barrer), Academic Press, London, **1982**.

[7] P. Lu, L. A. Villaescusas, M. A. Camblor, *Chem. Rec.* **2018**, *18*, 1-12.

[8] a) M. A. Camblor, L. A. Villaescusa, M. J. Díaz-Cabañas, *Top. Catal.* **1999**, *9*, 59-76; b) M. A. Camblor, P. A. Barrett, M. J. Díaz-Cabañas, L. A. Villaescusa, M. Puche, T. Boix, E. Perez, H. Koller, *Microporous*

Mesoporous Mater. **2001**, *48*, 11-22; c) J. Song, H. Gies, *Stud. Surf. Sci. Catal.* **2004**, *154A*, 295-300; d) S. I. Zones, R. J. Darton, R. Morris, S. J. Hwang, *J. Phys. Chem. B* **2005**, *109*, 652-661.

[9] a) A. Corma, M. J. Díaz-Cabañas, J. Jiang, M. Afeworki, D. L. Dorset, S. L. Soled, K. G. Strohmaier, *Proc. Natl. Acad. Sci.* **2010**, *107*, 13997-14002; b) T. Willhammar, A. W. Burton, Y. Yun, J. Sun, M. Afeworki, K. H. Strohmaier, H. Vroman, X. Zou, *J. Am. Chem. Soc.* **2014**, *136*, 13570-13573.

[10] C. Jo, S. Lee, S. J. Cho, R. Ryoo, *Angew. Chem.* **2015**, *127*, 12996-12999; *Angew. Chem. Int. Ed.* **2015**, *54*,12805-12808.

[11] a) W. Wan, J. Sun, J. Su, S. Hovmoller, X. Zou, *J. Appl. Cryst.* **2013**, *46*, 1863-1873; b) J. Li, J. Sun, *Acc. Chem. Res.* **2017**, *50*, 11, 2737-2745; c) J. Li, C. Lin, Y. Min, Y. Yuan, G. Li, S. Yang, P. Manuel, J. Lin, J. Sun, *J. Am. Chem. Soc.* **2019**, *141*, 4990-4996.

[12] M. M. J. Treacy, J. M. Newsam, M. W. Deem, *Proc. R. Soc. Lond. A* **1991**, *433*, 499-520.

[13] M. M. J. Treacy, M. W. Deem, DIFFaX. A computer program for calculating Diffraction Intensity from Faulted Crystals, v. 1.813, 19th May **2010**.

[14] W. Kabsch, *Acta. Cryst. D* **2010**, *66*, 125-132.

[15] G. M. Sheldrick, *Acta. Cryst. A* **2015**, *71*, 3-8.

[16] Ch. Baerlocher, A. Hepp, W. M. Meier, DLS-76. A Program for the Simulation of Crystal Structures by Geometric Refinement, Institute of Crystallography and Petrography, ETH, Zürich, **1977**.

[17] L. Tang, L. Shi, C. Bonneau, J. Sun, H. Yue, A. Ojuva, B.-L. Lee, M. Kritikos, R. G. Bell, Z. Bacsik, J. Mink, X. Zou, *Nature Mater.* **2008**, *7*, 381-385.

HPM-14, a New Germanosilicate Zeolite with Interconnected Extra-Large Pores Plus Odd-Membered and Small Pores

Supporting Information

Table of Contents

Experimental Procedures

S1. Experimental Section

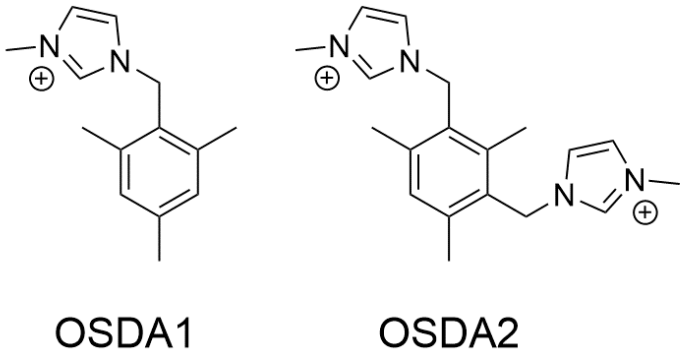

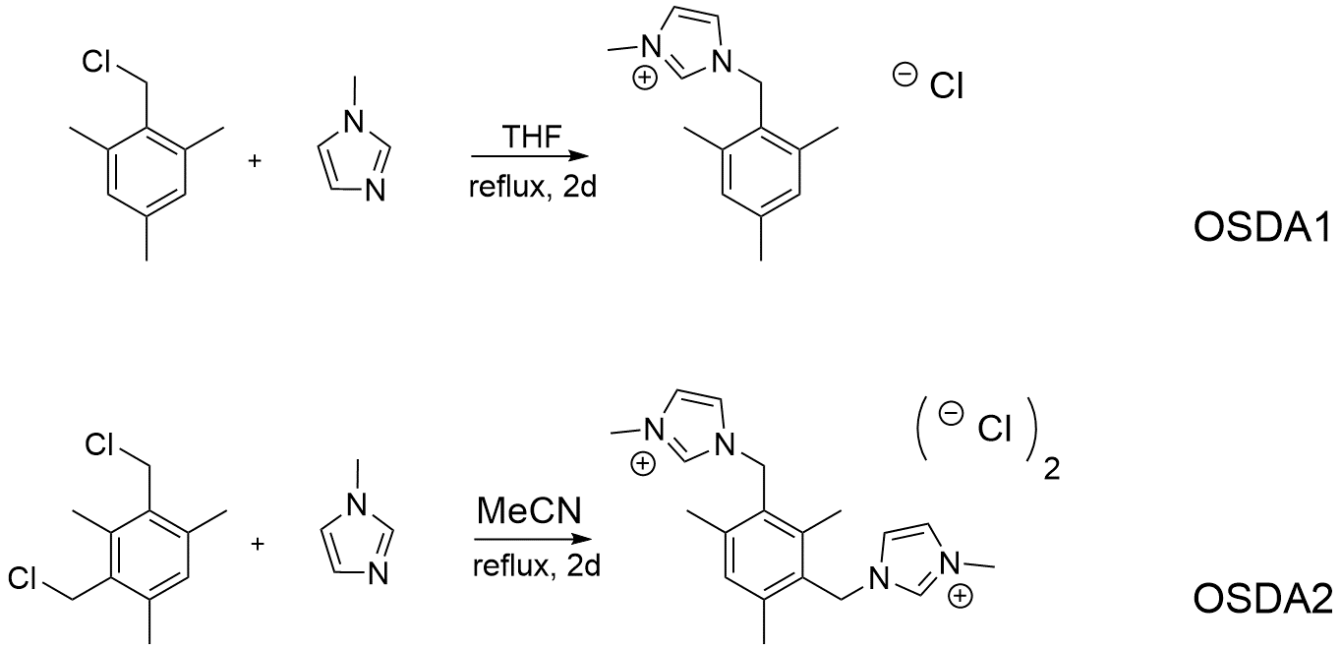

Scheme S1. Two OSDAs used for the synthesis of HPM-14 and their syntheses.

S1.1. Synthesis of OSDA1.
In a 500-mL, round-bottom flask, 25.00 g (148.2 mmol) 2-(chloromethyl)-1,3,5-trymethylbenzene and 14.08 g (171.5 mmol) 1-methylimidazole were solved into 300 mL THF. The solution was stirred overnight at r. t. and then refluxed for 2 d. At the end of the reaction, a large amount of white solid could be observed in the flask. After cooling down to r. t., the mixture was filtrated and then washed with 50 mL ethyl ether 3 times. The white solid was dried at 80 ^{o}C overnight to get OSDA1-Cl: 1-Methyl-3-(2',4',6'-trimethylbenzyl)imidazolium chloride (34.31 g, 136.8 mmol; yield 92.3 %). ^{1}H NMR (300 MHz, D_2O) δ 2.19 (s, 6H), 2.23 (s, 3H), 3.75 (s, 3H), 5.32 (s, 2H), 7.01 (s, 2H), 7.27 (t, 1H), 7.36 (t, 1H), 8.31 (m, 1H); ^{13}C NMR (300 MHz, D_2O) δ 140.3, 138.8, 135.4, 129.4, 125.9, 123.7, 121.9, 47.2, 35.7, 20.1, 18.4.

S1.2. Synthesis of OSDA2.
Changing the solvent from THF into acetonitrile, similar steps were performed on 17.35 g (79.90 mmol) 2,4-bis(chloromethyl)-1,3,5-trymethylbenzene and 14.82 g (180.5 mmol) 1-methylimidazole to get OSDA2-Cl: 1,1'-((2,4,6-trimethyl-1,3-phenylene)bis(methylene))bis(3-methylimidazolium) chloride (28.90 g, 75.78 mmol; yield 94.8 %). ^{1}H NMR (300 MHz, D_2O) δ 2.17 (s, 3H), 2.28 (s, 6H), 3.79 (s, 6H), 5.44 (s, 4H), 7.21 (s, 1H), 7.31 (t, 2H), 7.40 (t, 2H), 8.40 (m, 2H); ^{13}C NMR (300 MHz, D_2O) δ 140.8, 139.1, 135.4, 131.4, 127.8, 123.9, 121.9, 47.6, 35.8, 18.9, 14.7.

S1.3. Anion exchange.
33.22 g (141.8 mmol) OSDA1-Cl was solved into 250 mL deionized water. After totally solved with the help of ultrasound, the OSDA1-Cl solution was subjected to ion-exchange using a column filled with the hydroxide form of the resin Dowex Monosphere 550A. The OSDA1-OH solution was titrated with 0.1000 M HCl (aq.) to determine the real concentration of OSDA1-OH. The yield of the ion-exchange is 99% and Cl- could not be detected by $AgNO_3$ test.

A similar procedure was performed on OSDA2-Cl, to get OSDA2-OH (yield: 99%).

S1.4. Synthesis of Zeolite
A high-throughput synthesis method varying the OSDA/T, Ge/T (germanium fraction, marked as Ge_f) and H_2O/T molar ratios was used for the discovery of HPM-14 using OSDA1. More information could be found in Tab. S1. OSDA2 was also studied but under a more limited range of conditions. Here we provide two examples of gel preparation and zeolite synthesis: (1) for OSDA1: 0.7 SiO_2 : 0.3 GeO_2 : 0.5 OSDAOH : 0.5 HF : 5 H_2O at the rotation speed of 60 rpm at 160 ^oC for 7 days, and (2) for OSDA2: 0.4 SiO_2 : 0.6 GeO_2 : 0.4 $OSDA(OH)_2$: 0.8 HF : 5 H_2O at the rotation speed of 60 rpm at 160 ^oC for 6 days.

23.020 g OSDA1-OH (6.008 mmol, $[OH^-]$ = 0.261 mmol/g) and 0.37667 g (3.600 mmol) GeO_2 were added in a flask and stirred until a clear solution was obtained. Then, 1860 µL (8.330 mmol) TEOS (tetraethylorthosilicate) was added into the flask. The solution was stirred allowing ethanol and water to evaporate until the targeted amount of water was reached, then 228 µL (6.031 mmol, *c* = 26.45 mol/L) HF was added into the solution under stirring. After the solution changed into gel, the stirrer was removed and the gel transferred into a 30-mL autoclave. With a tumbling speed of 60 rpm, the gel was crystallized at 160 ^oC for 7 d. After finishing the crystallization, the sample in the autoclave was filtrated and washed with water (2 x 30 mL) and acetone (1 x 30 mL), and dried in an oven at 80 ^oC (0.778 g, Yield: 23.1%).

A similar procedure was performed using OSDA2-OH, with 26.686 g (9.660 mmol, $[OH^-]$ = 0.362 mmol/g) $OSDA2(OH)_2$, 0.75324 g (7.198 mmol) GeO_2, 1080 µL (4.837 mmol) TEOS and 363 µL (9.601 mmol, *c* = 26.45 mol/L) HF, under 160 ^oC for 6 d to get 0.788 g samples (Yield: 20.8%).

S2. Method of cRED Data Collection and Structure Solution of HPM-14
The cRED data were collected on 200kV JEOL JEM-2100 transmission electron microscope using the software *instamatic*. During the data collection, the goniometer was rotated continuously while the selected area ED patterns were captured from the crystal simultaneously by a quad hybrid pixel detector (Timepix). Eight datasets were collected on different crystals. The typical dataset for reconstruction is 381 ED patterns, which was recorded with tilt step of 0.23°, and the tilt range from -60.0° to 37.3°. The original RED data and reconstructed 3D reciprocal lattice are shown in Movies S1 and S2, respectively.

S3. Method of C_s-corrected HRSTEM Experiment of HPM-14
The HPM-14 framework was analyzed by means of spherical aberration-corrected (C_s-corrected) Scanning Transmission Electron Microcopy (STEM) combining the data acquired using an annular dark field (ADF) detector with an annular bright field (ABF) detector. Electron microscopy imaging was performed in a double spherical aberration corrected JEOL GrandARM operated at 300 kV.

S4. Other Characterization Methods
Powder X-ray diffraction (PXRD) patterns were obtained in a Bruker D8 Advance diffractometer with Cu Kα radiation (λ = 1.5418 Å). In situ PXRD patterns at various temperature were collected in a Panalytical X'Pert PRO Theta/Theta diffractometer with Cu Kα radiation. Field emission scanning electron micrographs (FE-SEM) and energy-dispersive X-ray spectroscopy (EDS) data were collected by FEI Nova NanoSEM 230. Multinuclear, *i.e.* ^{13}C, ^{19}F and ^{29}Si, magic angle spinning (MAS) solid state NMR spectra of as-made zeolite samples were performed at room temperature on a Bruker AV-400-WB equipment and the details have been given elsewhere.[S1] ^1H and ^{13}C liquid NMR spectra of D_2O solutions of as-made OSDAs were performed on a Bruker Avance III-HD Nanobay 300 MHz. CHN elemental analysis of as-made zeolite was carried out on a LECO CHNS-932 analyzer in order to determine the organic amount. Thermogravimetric (TG) analysis was performed in an SDT Q600 TA instrument under air flow (100 mL/min) heating from 25 ^oC to 1000 ^oC at a heating rate of 10 ^oC/min for the as-made OSDA (Fig. S16) and for the as-made zeolite (with or without a plateau at 140 ^oC to clearly distinguish water from OSDA losses, Fig. S15, S17).

S5. Method of DIFFAX Simulation
The diffraction patterns of intergrowths resulting from stacking faults along one direction can be calculated using the program DIFFaX.[S2] In DIFFaX, the stacking disorder must occur along [001], and hence for HPM-14, a change of coordinates is necessary. The stacking layer has been conveniently described as half the unit cell along [001] direction of the orthorhombic polymorph B after a change of coordinates (*x*' = *y*, *y*' = *z*, *z*' = *x*). Successive layers need to be rotated 180º around [100] direction or, equivalently, translated by 0.5*a* along that direction. A translation by ±1/4*b* along [010] direction is also needed. When translations along [010] direction occur always in the same direction, *i.e.* always by +1/4*b* or always by -1/4*b*, an AAAA

stacking that constitutes the monoclinic polymorph HPM-14A is obtained, whereas alternate +1/4*b*, -1/4*b*, +1/4*b*, -1/4*b* translations produce the ABAB orthorhombic polymorph HPM-14B.

In order to compare with the PXRD pattern of the calcined material, the dimensions of the orthorhombic unit cell were refined using eight reflections of the pattern shown in the black curve in Fig. S6 and the program Unit Cell.[S3] After halving along *c*-axis, the basic layer used in DIFFaX has dimensions *a* = 24.02474, *b* = 10.32714, *c* = 11.27662 Å. The Si and O atomic positions were obtained from the orthorhombic polymorph after geometrical distance least squares fitting using DLS-76.[S4] The patterns of the end members simulated with DIFFaX agree well with those simulated with VESTA for the pure polymorphs (see Fig. S6). Close inspection of the simulated patterns corresponding to intergrowths revealed that the most significant changes in the patterns occur in the 10-15º 2θ region. There, orthorhombic reflections around 10.1º and 13.8º disappear while the peaks at 11.2º and 12º move close to each other and finally merge as the monoclinic polymorphs becomes more predominant. Additionally, the orthorhombic reflections at 12.2º and 13.8º become broader and approach to each other, finally merging in a new reflection at 12.7º.

Results and Discussion

S6. Synthesis Discussion

With OSDA1, zeolite HPM-14 could be synthesized from a gel with composition 0.7 SiO_2 : 0.3 GeO_2 : 0.5 OSDAOH : 0.5 HF : 5 H_2O under rotation at 160 ºC for 5-9 days (Entries 6a-6c in Tab. S1). At the same gel composition, **ITT**, a zeolite with 18×10×10 MR pores, would eventually crystallize with longer time (Entries 6d-6f). This implies **ITT** is more stable than HPM-14 despite its lower framework density, which is another example of a phase transformation from a denser framework to a more open one.[S5] When decreasing or increasing the water content at the same Ge_f (0.3), there is a strong competition from other zeolite phases, *i.e.* **ITT** (Entries 4, 5a-5d) and **UOS** (Entries 7a-7d, 8), respectively. This tendency follows the experimental observation that as the H_2O/T ratio increases the framework density increases (framework density in T/1000Å^3 units: **ITT** 12.4, HPM-14 14.1, **UOS** 17.9; Villaescusa's rule).[S6] Ge_f is also an important factor to determine the product phase. With a higher Ge content (Ge_f = 0.5), the main phases are NUD-1 and **ITT** (Entry 1); with a lower Ge content, they are **ITT** (Entries 9a-9d; Ge_f = 0.2) or mainly amorphous with traces of HPM-14 (Entries 10a-10e, 11; Ge_f = 0.15) or **UOS** (Entry 12; Ge_f = 0.15) depending on the H_2O/T ratio. At even lower Ge_f (0.03), the OSDA fails to direct any crystalline phase (Entries 13, 14, 15). Finally, changing the OSDA content (OH^-/T) has a limited impact on the product phase (Entries 6a-6f, 21a-21c, 32) in the tested ranges (0.5-1.2).

OSDA2 was also studied under a more limited range of conditions and it produced HPM-14 from gel compositions with high Ge_f (> 0.5). A recipe with OSDA2 yielding a pure and well crystallized phase uses a gel composition of 0.4 SiO_2 : 0.6 GeO_2 : 0.4 $OSDA(OH)_2$: 0.8 HF : (4-5) H_2O under rotation at 160 ºC for 5-7 days. Competing phases in the synthesis with OSDA2 are **IRR**, **-ITV**, **UOS** and NUD-1.

S7. Physicochemical Characterization

A zeolite HPM-14 sample with relatively low Ge_f (0.3) synthesized using OSDA1 is used for all the characterization. Scanning electron microscope (SEM) image showed that HPM-14 crystals are needle-like, with a size close to 40×5×5 µm^3 (Fig. S8), which is perfect for data collection of electron diffraction. The PXRD pattern of the as-made sample (Fig. S9a) showed not only sharp peaks but also broad ones at, for example, 11.4º and 12.7º, indicating that the crystals contain disorder or defects. *In situ* PXRD shows that HPM-14 with relatively low Ge_f (0.3) was stable up to 540 °C under dry air (Fig. S10), indicating that permanent pores of HPM-14 could be generated by calcination. However, another HPM-14 sample with higher Ge_f (0.6) was totally decomposed at 550 ºC under dry air (Fig. S11), showing that the stability of HPM-14 dramatically depends on the Ge content. Hence, an HPM-14 sample of Ge_f = 0.3 was calcined at 500ºC for 3 hours and its pattern in Fig. S9b will be compared with DIFFaX simulations.

The ^{29}Si solid state magic angle spinning nuclear magnetic resonance (MAS NMR) spectrum showed a broad and featureless single peak at δ = -105.1 ppm (Fig. S12) with no resolution of crystallographic sites or $Si(OT)_4$ species (T = Si, Ge). In Fig. S13, ^{19}F solid state MAS NMR spectrum showed 2 types of F signal at δ = -9.59 and -123.9 ppm. The first one is assigned to F^- anions in [Si, Ge]-*d4r* of type III, *i.e.* containing Ge pairs but no Ge with three neighboring Ge atoms.[S7] The second signal is assigned to $[SiF_x(OH)_{6-x}]^{2-}$ impurity species or to a surface fluorosilicate species.[S8] The solid state NMR spectrum of as-made HPM-14 (Fig. S14a) matched well with the ^{13}C liquid NMR spectrum of as-made OSDA1 (Fig. S14b), which proves that the OSDA in the as-made zeolite is essentially intact. Elemental analysis also supported this point as the experimental C/N mole ration (7.04) matched well the calculated one (7, Tab. S3). Energy dispersive spectroscopy (EDS) analyses showed that individual crystallites have variable Ge_f (0.5-0.6), while analysis of larger areas provided lower values, likely due to the presence of more siliceous amorphous phases. In the thermogravimetric (TG) analysis of as-made HPM-14 under a steady increment of 10 ºC/min from r. t. to 1000 ºC, it was complicated discerning water and OSDA losses (Fig. S15). A TG analysis showed that OSDA1 begins to decompose/oxidize from around 180 ºC (Fig. S16), hence a second TG analysis on as-made HPM-14 was done including a 3-hour plateau at 140 ºC (red curve in Fig. S17). The resulting TG curve (black curve in Fig. S17) gave a 1.66% weight loss up to 140 ºC (H_2O value calculated from CHN analysis: 3.58%), and 17.60% between 140 ºC and 1000 ºC (OSDA calculated value: 16.39%), respectively. The discrepancies suggest the existence of T-OH connectivity defects that would be annihilated at temperatures well above 140 ºC. We note anyway that, at least for small, medium but even large pore zeolites, the thermal processes associated to calcination may be complex and obscure the interpretation of the TG analyses.[S9]

Supporting Tables and Figures

Tab. S1 OSDA1 High-throughput synthesis results.[1]

Entry	Synthesis Condition				Product	Entry	Synthesis Condition				Product
	OH^-/T	Ge/T	H_2O/T	*t*(d)			OH^-/T	Ge/T	H_2O/T	*t*(d)	
1	0.5	0.5	2.5	7	NUD-1 + **ITT**	16a	0.8	0.6	10	2	IC
2	0.5	0.5	5	7	NUD-1 + HPM-14	16b				4	HPM-14
3	0.5	0.5	10	7	HPM-14 + GeO_2	16c				6	HPM-14 + **UOS**
4	0.5	0.3	2.5	7	**ITT**	17	0.8	0.5	2.5	7	**ITT**
5a	0.5	0.3	4.5	5	**ITT** + HPM-14	18	0.8	0.5	5	7	NUD-1 + **ITT**
5b				9	**ITT** + HPM-14	19a	0.8	0.5	10	3	IC
5c				12	NUD-1 + **ITT**	19b				4	IC
5d				16	NUD-1 + **ITT**	19c				7	HPM-14
6a	0.5	0.3	5	5	HPM-14	19d				10	HPM-14 + **UOS**
6b				7	HPM-14	19e				17	HPM-14 + **UOS**
6c				9	HPM-14	20	0.8	0.3	2.5	7	**ITT**
6d				12	HPM-14 + **ITT**	21a	0.8	0.3	5	7	HPM-14
6e				14	**ITT**	21b				10	HPM-14 + **ITT**
6f				16	**ITT**	21c				14	HPM-14 + **UOS**
7a	0.5	0.3	5.5	5	HPM-14	22	0.8	0.3	10	7	**UOS**
7b				9	HPM-14 + **UOS**	23	0.8	0.15	2.5	7	Am
7c				12	HPM-14 + **UOS**	24	0.8	0.15	5	7	Am
7d				16	HPM-14 + **UOS**	25	0.8	0.15	10	7	**UOS** + Am
8	0.5	0.3	10	7	**UOS**	26	0.8	0.03	2.5	7	Am
9a	0.5	0.2	2.5	7	**ITT**	27	0.8	0.03	5	7	Am
9b				10	**ITT**	28	0.8	0.03	10	7	Am
9c				14	**ITT**	29	1.2	0.5	2.5	7	**ITT**
9d				20	**ITT**	30	1.2	0.5	5	7	**ITT**
10a	0.5	0.15	2.5	5	Am	31	1.2	0.5	10	7	HPM-14
10b				7	HPM-14 + Am	32	1.2	0.3	5	7	HPM-14
10c				9	Am						
10d				15	HPM-14 + Am						
10e				25	Am						
11	0.5	0.15	5	7	HPM-14 + Am						
12	0.5	0.15	10	7	**UOS** + Am						
13	0.5	0.03	2.5	7	Am						
14	0.5	0.03	5	7	Am						
15	0.5	0.03	10	7	Am						

(1) All the OH^- is provided by the OSDA solution and the HF/OH^- ratio is always 1. A "+" refers to the mixture of two phases. **ITT** and **UOS** are ZFT codes.[S10] "Am" and "IC" refer to amorphous and ill-crystallized phases, respectively.

Tab. S2 cRED Experimental parameters of HPM-14.

Identification code	HPM-14
Tilt range	-60.0° ~ 37.30°
Tilt step	0.23°
Wavelength	0.0251 Å
Exposure time/frame (s)	0.5
Total data collection time (s)	217
No. of frames	381
Program for data procession	*XDS*
Program for structure determination	ShelxT
Resolution	0.80 Å
Completeness	70.7%
R_{int}	0.369
No. of unique reflections	7952

Tab. S3 C, H, N chemical analyses of as-made OSDA1-HPM-14

Experimental Weight Amount (*wt*%)			Experimental Mole Ratio		Theoretical Mole Ratio	
N	C	H	C/N	H/N	C/N	H/N
1.96	11.84	1.74	7.04	12.34	7	9.5

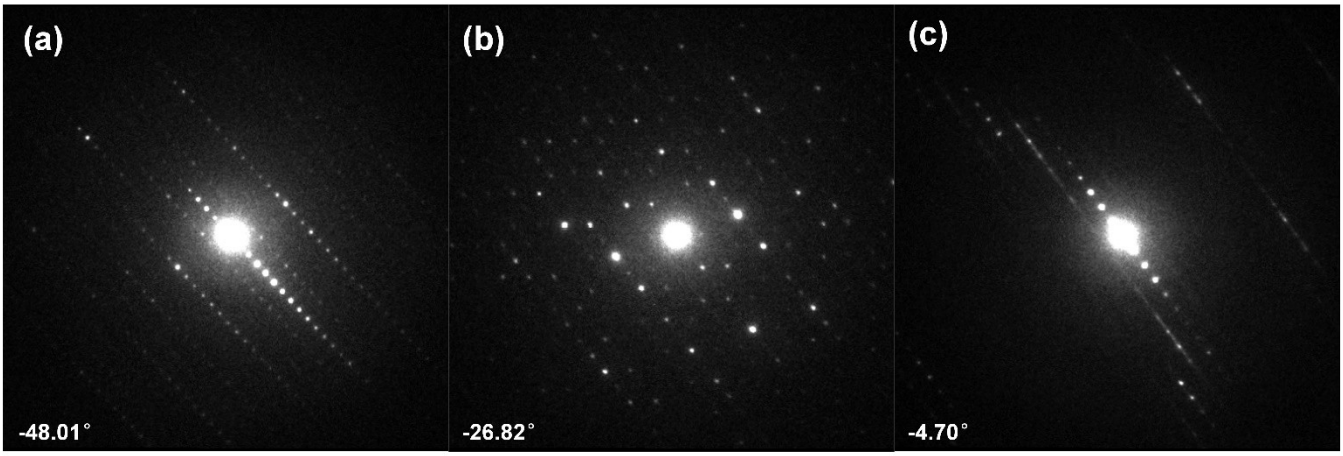

Fig. S1 Typical ED patterns under different tilt angle during cRED data collection, with tilt angle of (a) -48.01°, (b) -26.82°, and (c) -4.70°.

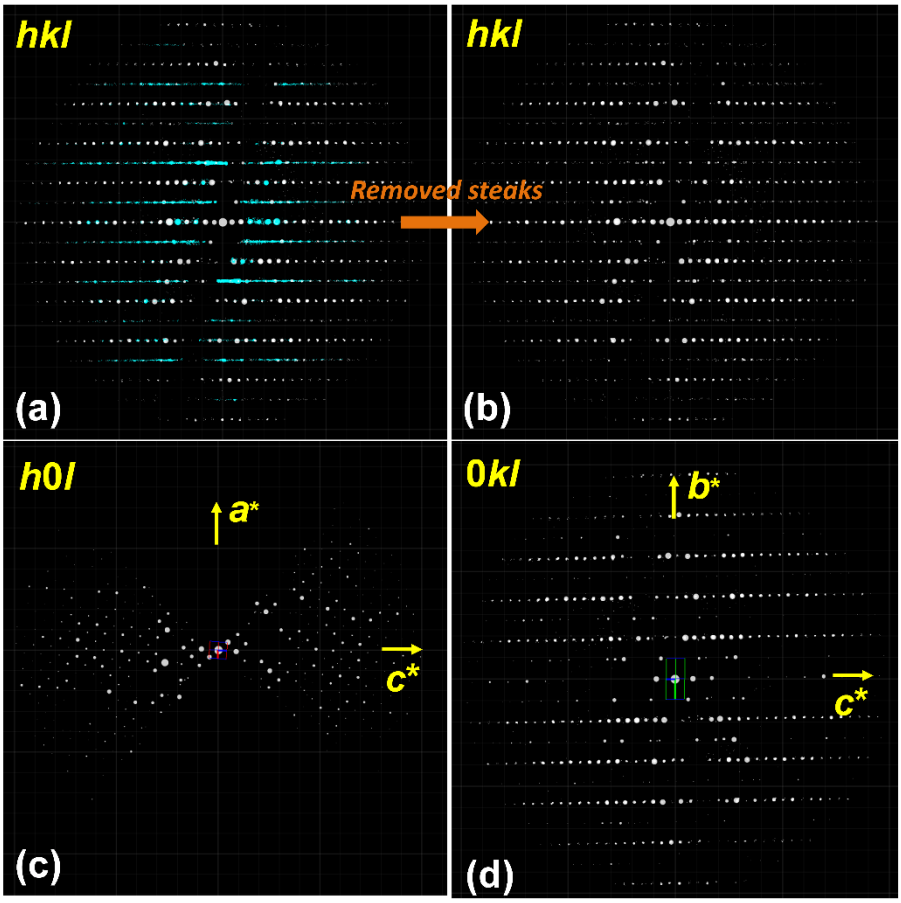

Fig. S2 Reconstructed 3D cRED data of HPM-14 indexed with orthorhombic symmetry: (a) 3D reciprocal lattice with streaks, (b) 3D reciprocal lattice after removing streaks, and selected planes in the reciprocal lattice and corresponding to *h*0*l* (c), 0*kl* (d). The reflection conditions can be obtained as: *h*0*l*: $h + l = 2n$, *hk*0: $h = 2n$. Owing to the streak, some reflections violate the reflection conditions.

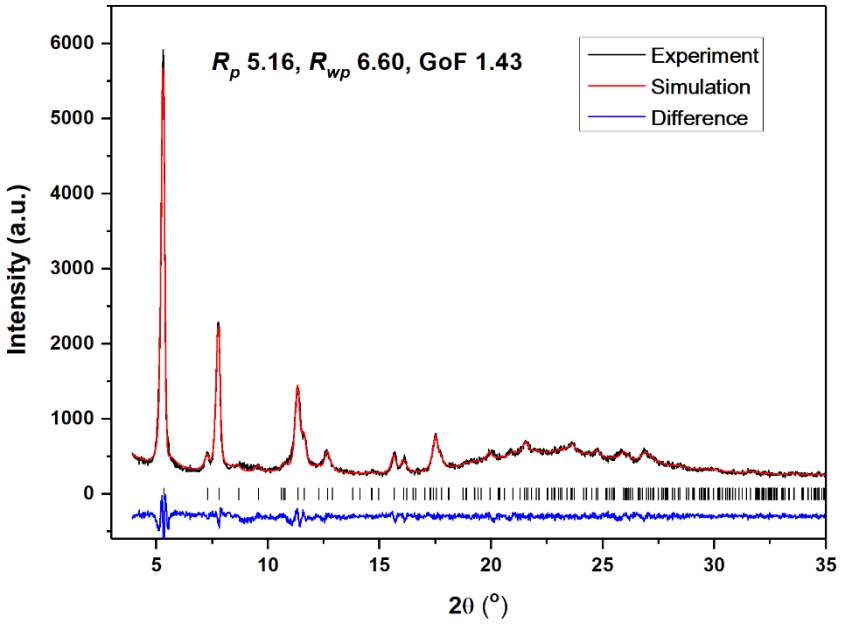

Fig. S3 Lebail fitting plot for calcined HPM-14 with the unit cell parameters and space group from monoclinic phase (HPM-14A). The curves in color black, red, and blue are experimental, simulated, and difference profiles, respectively.

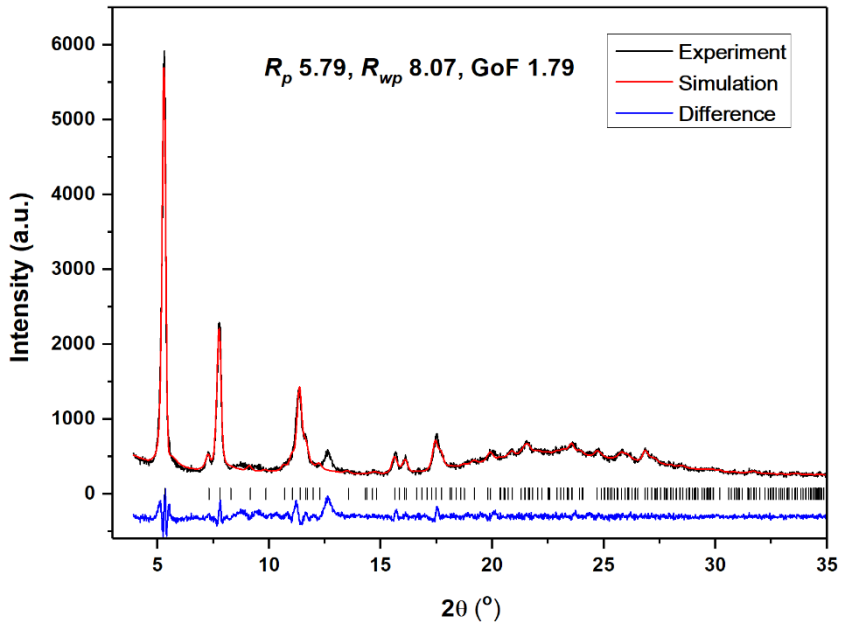

Fig. S4 Lebail fitting plot for calcined HPM-14 with the unit cell parameters and space group from orthorhombic phase (HPM-14B). The curves in color black, red, and blue are experimental, simulated, and difference profiles, respectively.

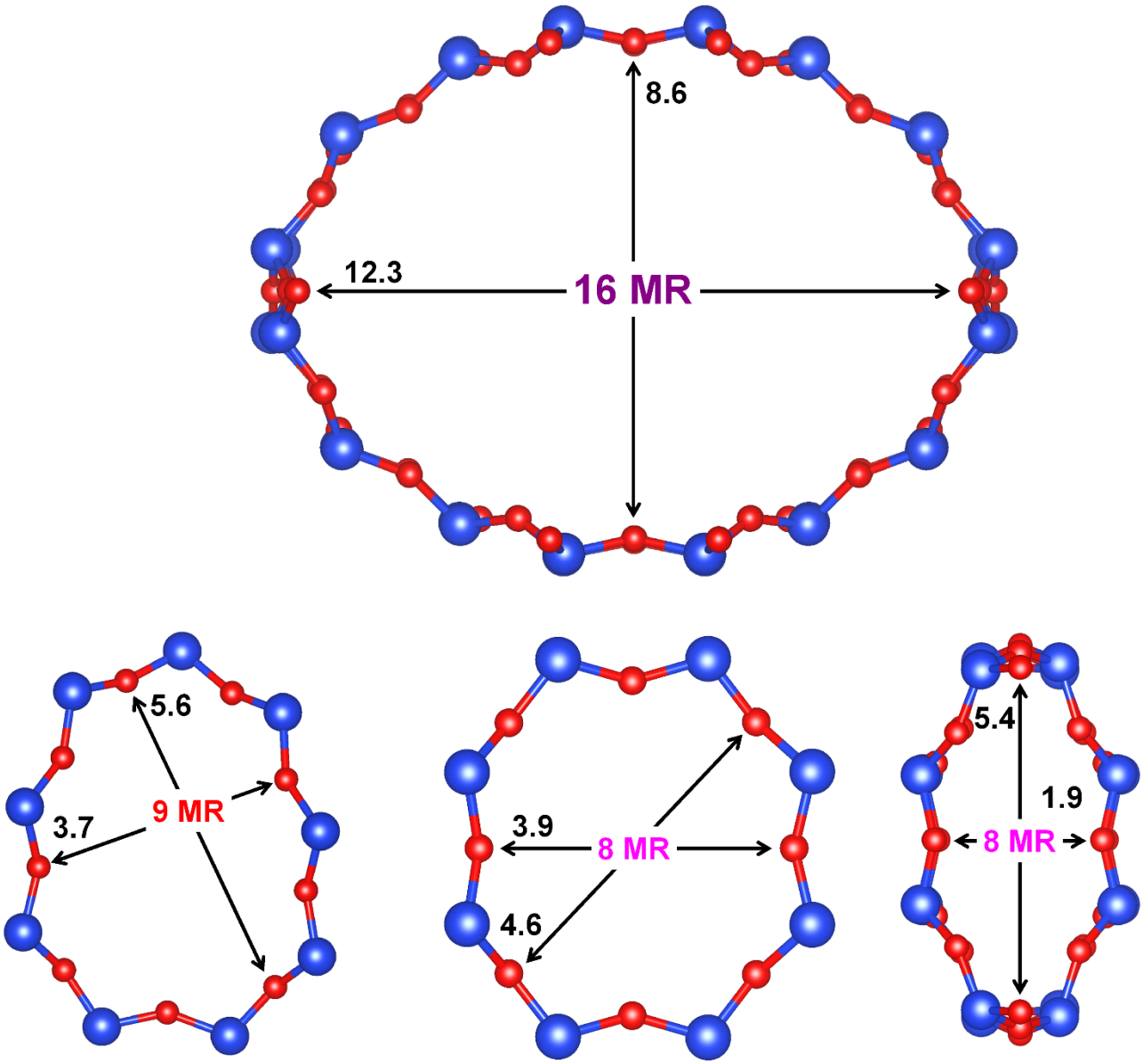

Fig. S5 Limiting rings of 16, 9 and 8 MR in the framework of HPM-14 (unit: Å)

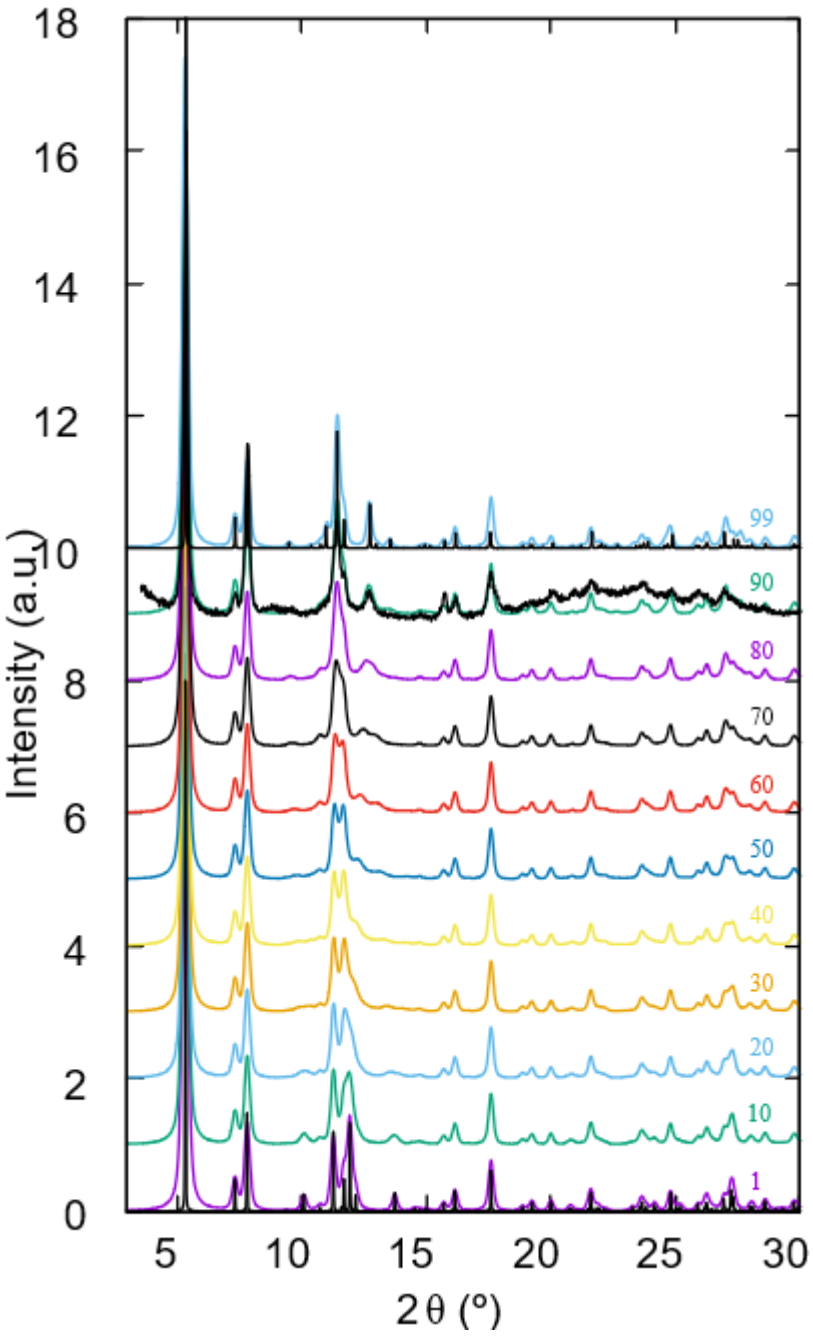

Fig. S6 DIFFaX simulations of powder patterns of a series of intergrown HPM-14B (bottom) and HPM-14A (top) with the percentage of polymorph A labelled near each trace. The bottom and top sharp black patterns correspond to the simulation of the pure orthorhombic and monoclinic end members calculated by VESTA.[S11] The black noisy pattern close to the 90/10 HPM-14A/B simulation is the experimental pattern of a calcined HPM-14 sample.

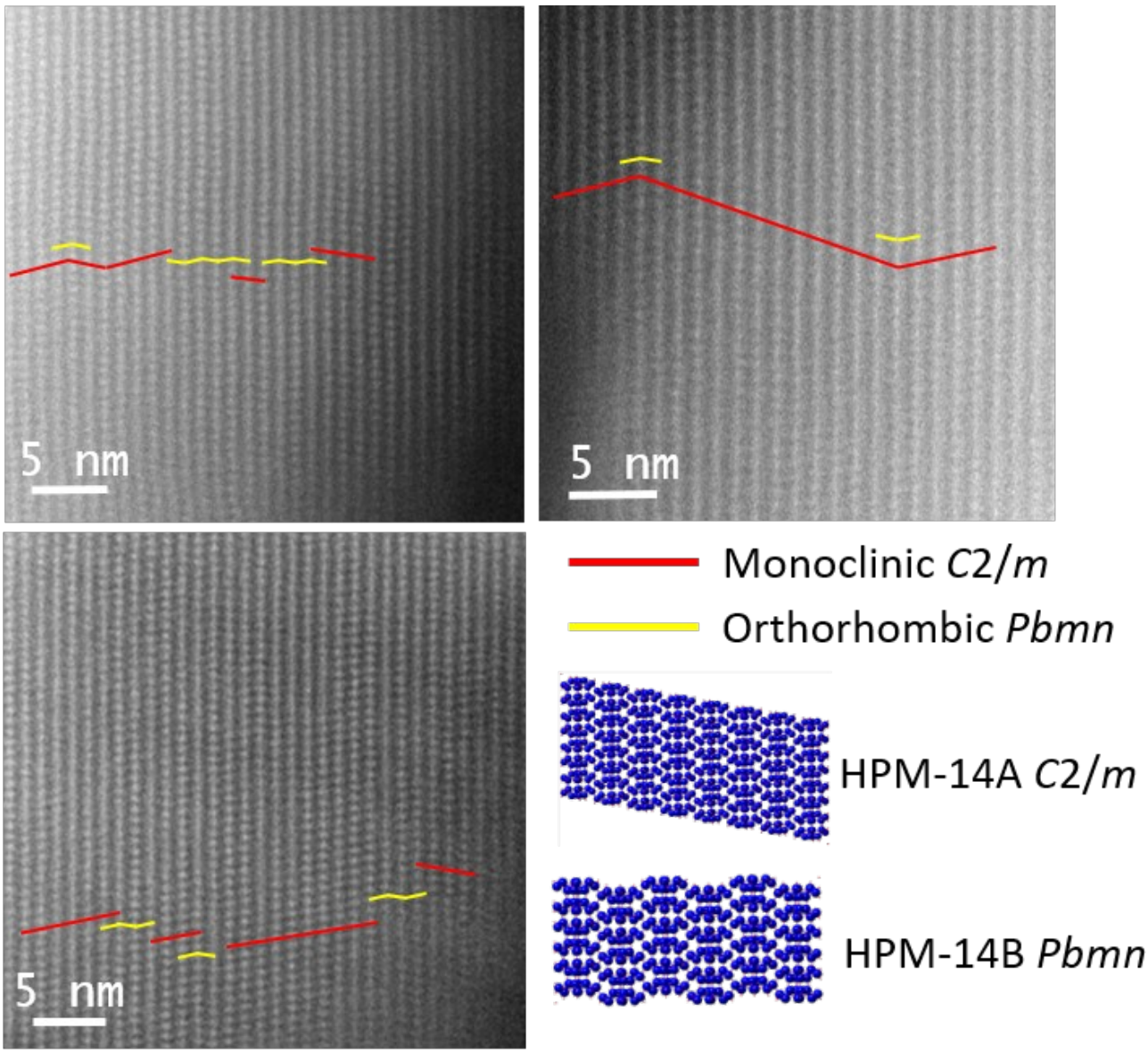

Fig. S7 Selected HRTEM images of HPM-14, showing the predominance of polymorph A in HPM-14. The polymorphs A and B are shown in red and yellow lines, respectively, and the models of two polymorphs with the Si and O represented in blue and red spheres, respectively.

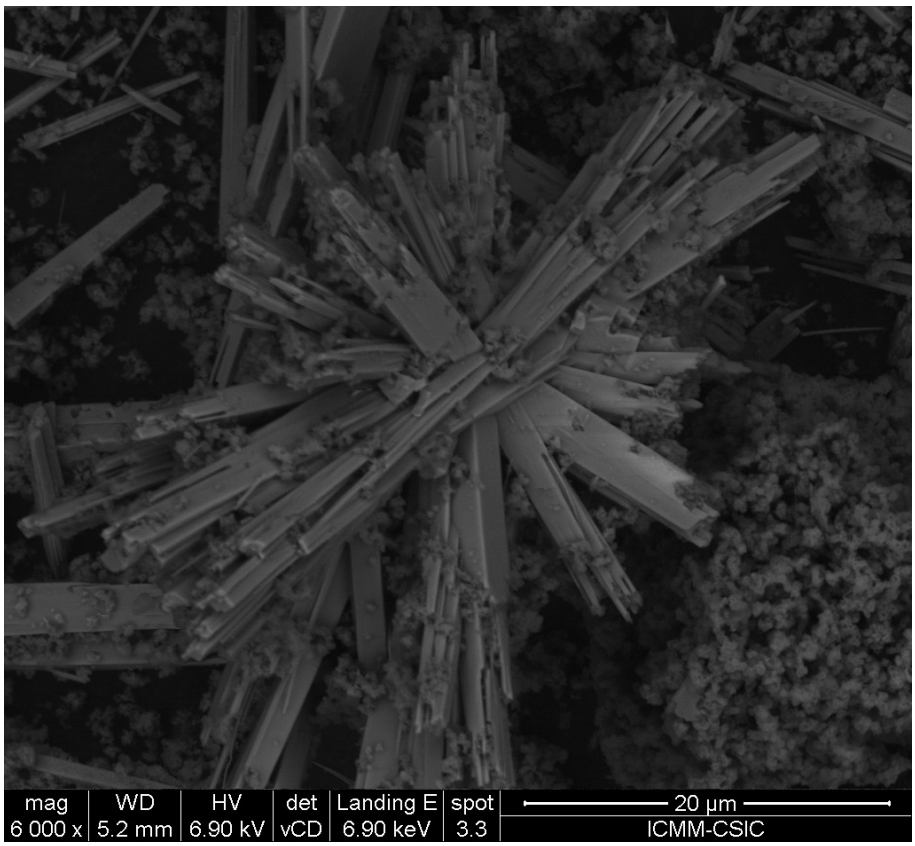

Fig. S8 FE-SEM image of as-synthesized HPM-14

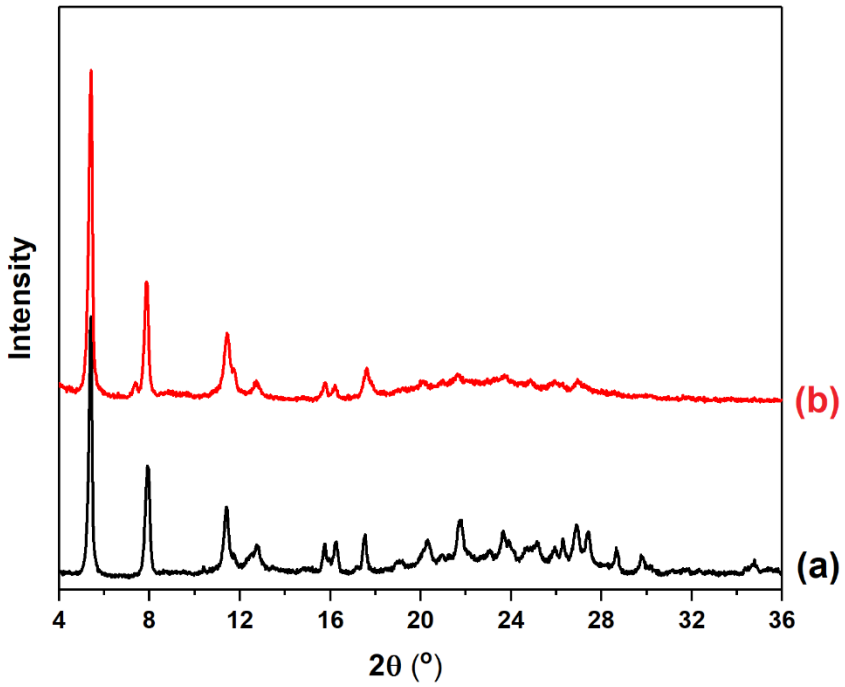

Fig. S9 PXRD patterns of (a) as-made and (b) calcined HPM-14

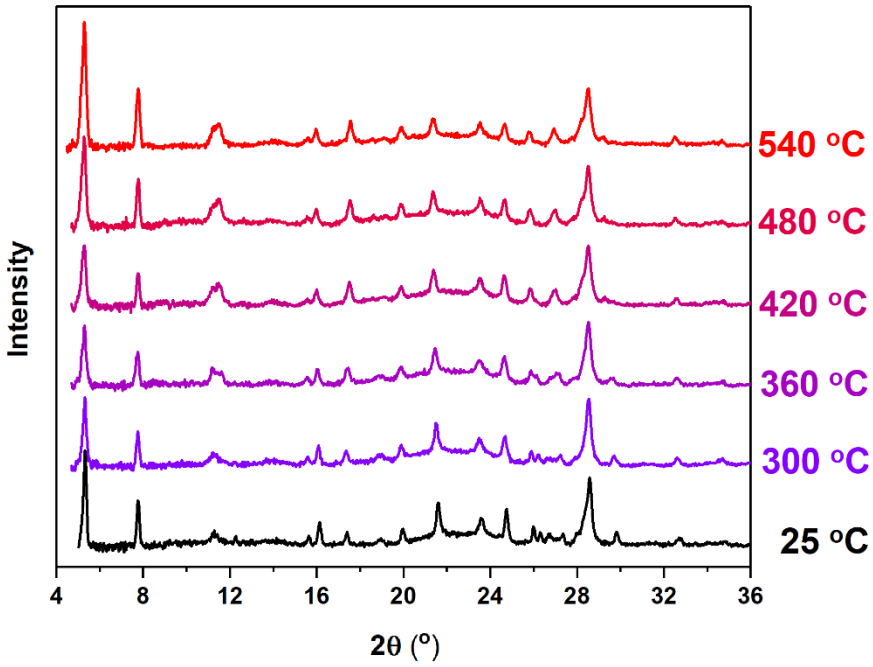

Fig. S10 *In situ* PXRD patterns of HPM-14 (Ge_f = 0.3) at various temperatures

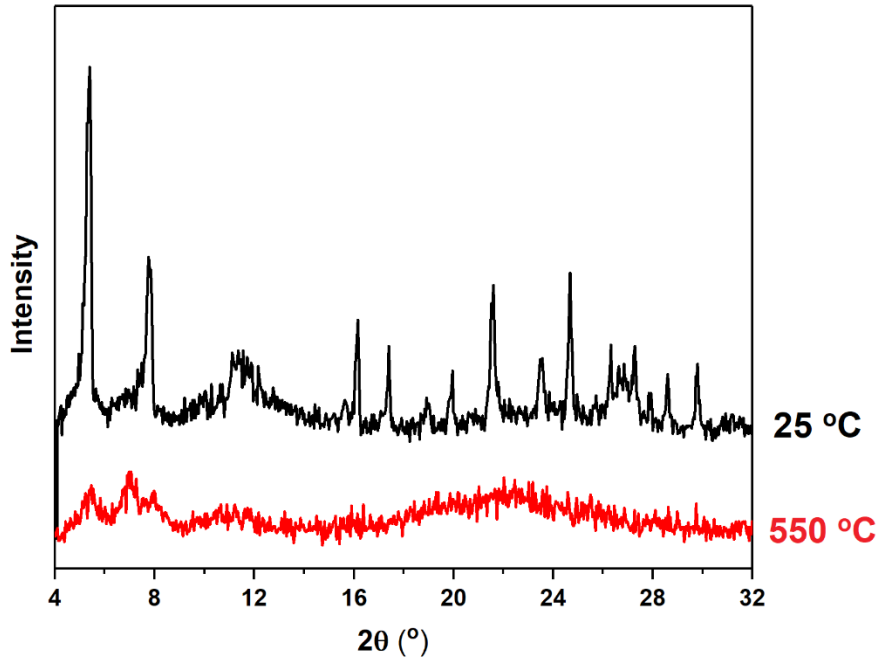

Fig. S11 *In situ* PXRD patterns of HPM-14 (Ge_f = 0.6) at various temperature

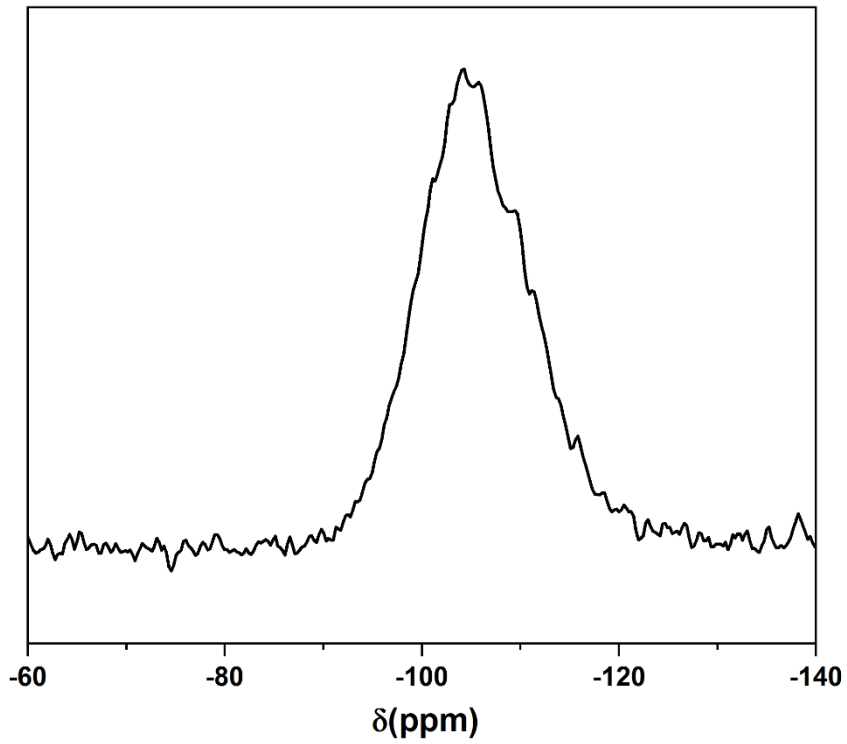

Fig. S12 ^{29}Si solid state MAS NMR spectrum of as-made HPM-14

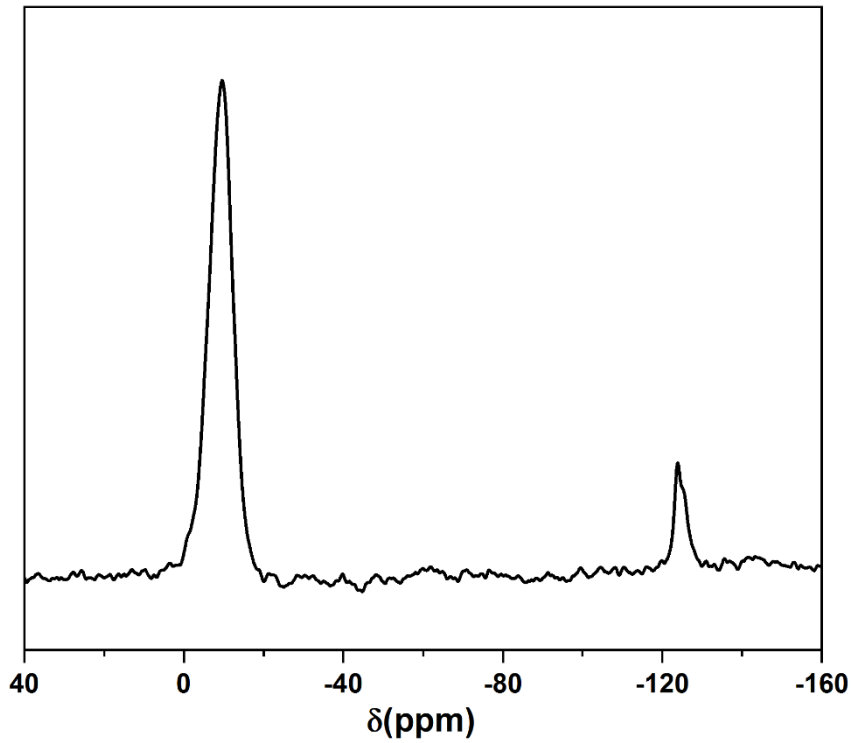

Fig. S13 ^{19}F solid state MAS NMR spectrum of as-made HPM-14

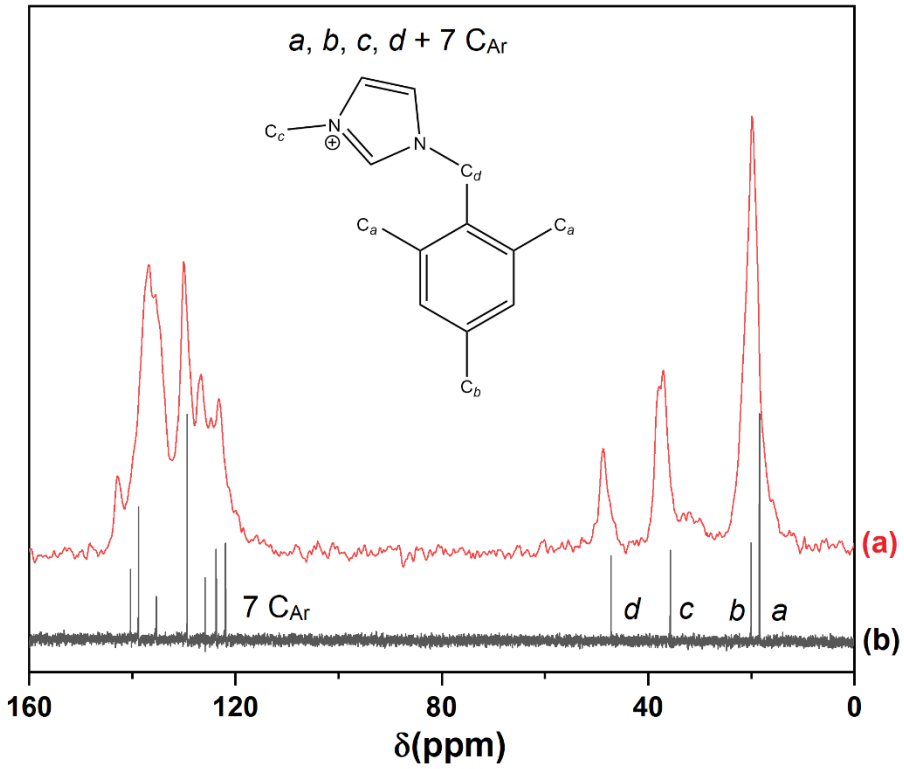

Fig. S14 (a) ^{13}C solid state NMR spectrum of OSDA1-HPM-14 and (b) ^{13}C liquid NMR spectrum of OSDA1

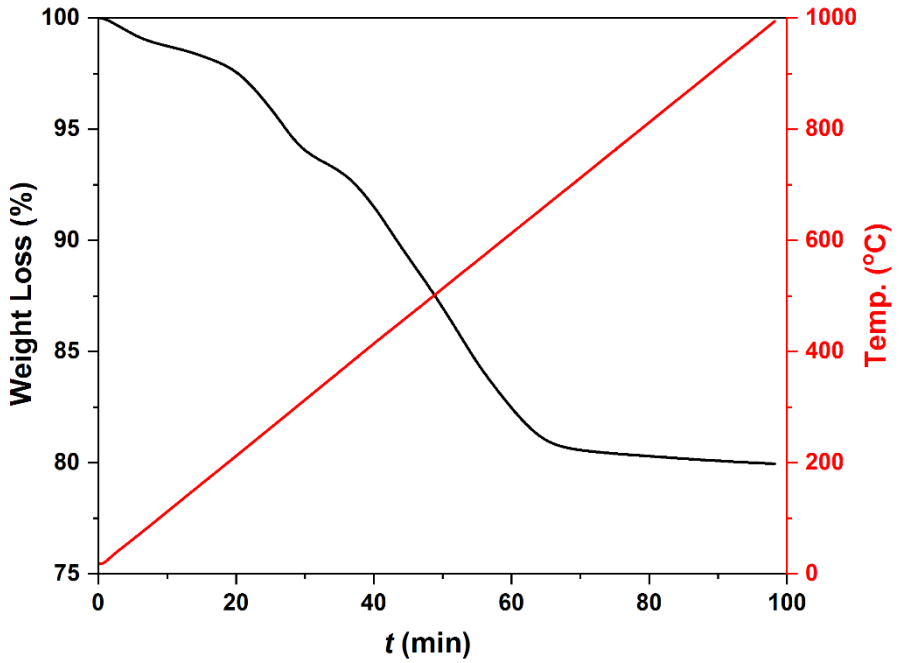

Fig. S15 Weight loss curve of HPM-14 (black) under a steady increment of temperature of 10 °C/min (red)

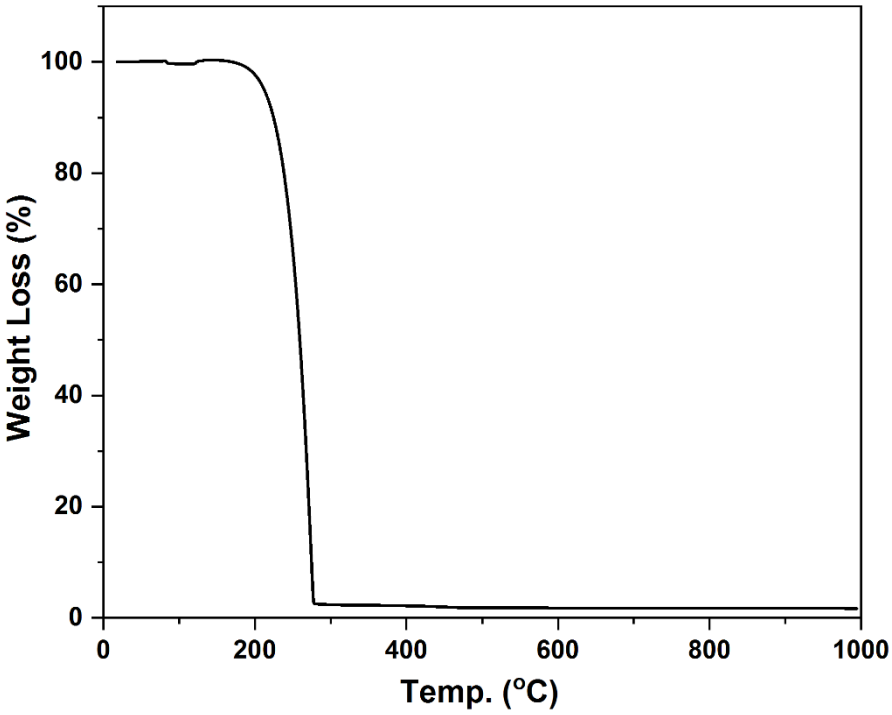

Fig. S16 TG curve of as-made OSDA1 during a steady increment of temperature of 10 °C/min.

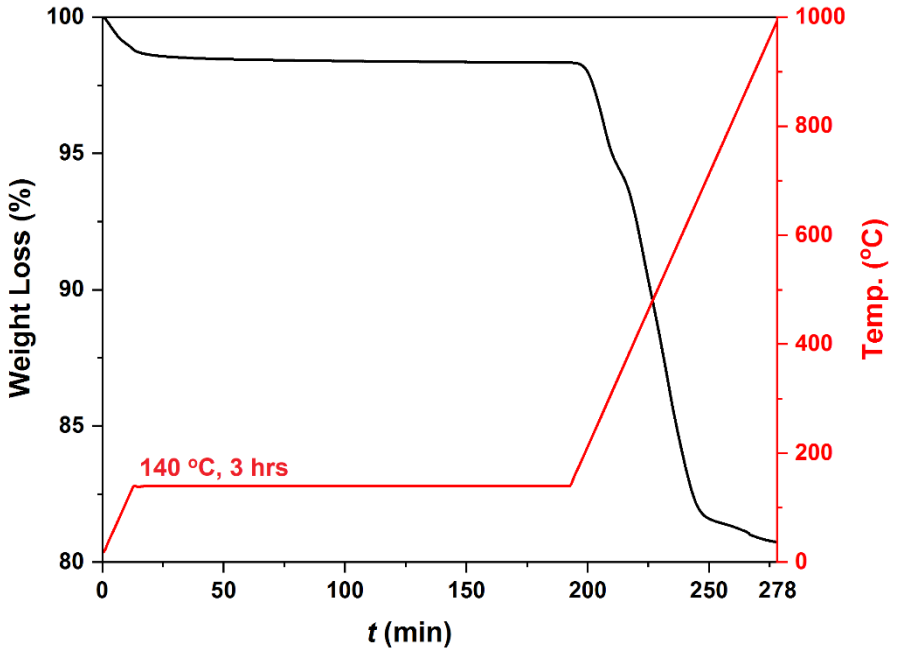

Fig. S17 Weight loss curve of HPM-14 (black) under a temperature rise program (red, a plateau at 140 °C for 3 hrs) designed to distinguish water and OSDA losses

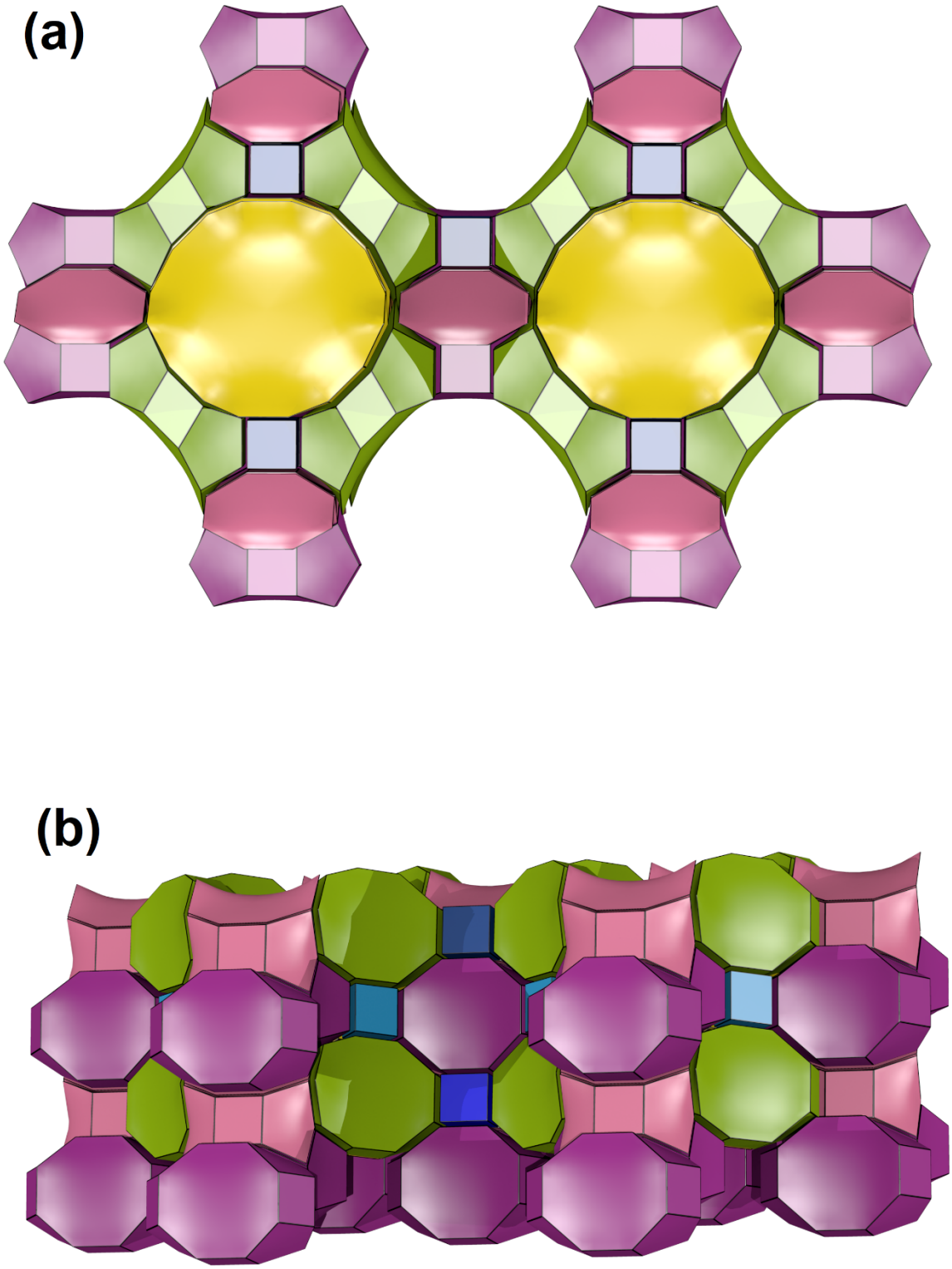

Fig. S18 Tilings of HPM-14: (a) showing the 16MR and 8MR along *c*-axis and (b) showing the 2D 9MR undulating channel and the 1D 8MR straight channel that are perpendicular to the 16MR channel. Various tilings are shown in color: yellow for [$4^2.5^2.8.16^2$] (16MR channel), green for [$4^4.5^6.9^2$] (9MR channel, also called *t-sof*-2 in the IZA zeolite database)[S10], pink for [$4.5^2.8^2$] (1st 8MR channel along *c*-axis), violet for [$4^4.5^6.8^3$] (2nd 8MR channel along *a*-axis), light blue and blue for two topologically different types of *d4r* [4^6], respectively.

References

[S1] A. Rojas, E. Martínez-Morales, C. M. Zicovich-Wilson, M. A. Camblor, *J. Am. Chem. Soc.* **2012**, *134*, 2255-2263.

[S2] a) M. M. J. Treacy, J. M. Newsam, M. W. Deem, *Proc. R. Soc. Lond. A* **1991**, *433*, 499-520; b) M. M. J. Treacy, M. W. Deem, *DIFFaX. A computer program for calculating Diffraction Intensity from Faulted Crystals*, v. 1.813, **19th May 2010**.

[S3] J. B. Holland, S. A. T. Redfern, *Mineral. Mag.* **1997**, *61*, 65-77.

[S4] Ch. Baerlocher, A. Hepp, W. M. Meier, *DLS-76. A Program for the Simulation of Crystal Structures by Geometric Refinement*, Institute of Crystallography and Petrography, ETH, Zürich, **1977**.

[S5] a) C. M. Zicovich-Wilson, F. Gándara, A. Monge, M. A. Camblor, *J. Am. Chem. Soc.* **2010**, *132*, 3461-3471; b) A. Rojas, E. Martínez-Morales, C. M. Zicovich-Wilson, M. A. Camblor, *J. Am. Chem. Soc*. **2012**, *134*, 2255-2263, c) P. Lu, L. Gómez-Hortigüela, L. Xu, M. A. Camblor, *J. Mater. Chem. A* **2018**, *6*, 1485-1495.

[S6] a) M. A. Camblor, L. A. Villaescusa, M. J. Díaz-Cabañas, *Top. Catal.* **1999**, *9*, 59-76; b) M. A. Camblor, S. B. Hong in *Porous Materials* (Eds.: D. W. Bruce, D. O'Hare, I. R. Walton), Wiley, Chichester, **2011**, pp. 265-325.

[S7] R. T. Reus, S. R. G. Balestra, S. Hamad, R. Bueno-Perez, A. R. Ruiz-Salvador, S. Calero, M. A. Camblor, *J. Mater. Chem. A* **2018**, *6*, 15110-15122.

[S8] a) J. H. Kang, D. Xie, S. I. Zones, M. E. Davis, *Chem. Mater.* **2020**, *32*, *5*, 2014-2024; b) P. Lu, L. Gómez-Hortigüela, M. A. Camblor, *Chem. Eur. J.* **2019**, *25*, 1561-1572

[S9] L. A. Villaescusa, M. A. Camblor, *Chem. Mater.* **2016**, *28*, *20*, 7544-7550.

[S10] Ch. Baerlocher, L. B. McCusker, *Database of Zeolite Structures*: http://www.iza-structure.org/databases/, access on **March 8th, 2020**.

[S11] K. Momma, F. Izumi, *J. Appl. Crystallogr*. **2011**, *44*, 1272-1276.

Author Contributions

Z.R.G., C.L. and M.A.C. designed the synthesis experiments, Z.R.G. performed the syntheses, J.L. and J.S. solved the structure, A.M. performed the C_s-STEM, M.A.C. performed the DIFFaX simulations, Z.G. and M.A.C. conducted the physicochemical characterization and prepared the manuscript. All the authors discussed the results and commented and revised the manuscript.